JOURNAL OF MATERIALS SCIENCE 32 (1997) 4133–4148

Synthesis, magnetic properties and formalism of magnetic properties of high-quality refined $Nd_2Fe_{14}B$ powders for permanent magnet devices

S. RAM*
Institute of Metal Research, Technical University of Berlin, Hardenbergstraße-36, D-10623, Berlin, Germany

Stable $Nd_2Fe_{14}B$ powders of refined grain size of 0.1–1.0 μm were prepared using a combination of the rapid quenching (of the melt into thin ribbons), mechanical attrition and grain-surface passivation (or surface hardening) and coating by a thermally rigid, adhesive and corrosion-proof material in air. The ribbons (of 15–30 μm thickness) were cut, crushed and milled under H_2 gas at approximately 1 bar and room temperature to give hydrided $Nd_2Fe_{14}BH_x$, $x \lesssim 5$, flakes of 1–5 μm sizes, which are brittle and easily obtained in powder form by high-energy ball milling. The interstitial H atoms in the hydride sample were desorbed by slowly heating (5 °C min^{-1}) the sample between 25 and 600 °C in N_2 gas (which helps the desorption of the H atoms without decomposition of the sample) in a reactor and then pumping off the total gas at 600 °C. The H-desorbed specimen, when annealed at 600–800 °C under a dynamic vacuum, results in a refined powder, showing a characteristically high remanence, J_r of 9–12 kG, together with a high intrinsic coercivity, H_{ci}, of 10–28.3 kOe, depending on the size and surface structure of the grains. This powder is highly pyrophoric and catches fire in open air but can be stabilized by passivating and coating the grain surfaces with a mixture of carbon, AlN and Nd_2O_3 by milling the mixture in a suitable organic liquid (to allow the additives to adhere the sample without excess oxidation) followed by annealing at an elevated temperature in N_2 gas at approximately 1 bar. In this process, the separated $Nd_2Fe_{14}B$ grains acquire a thin nitride–carbide (probably amorphous) stabilized surface passivation layer which prevents further oxidation of the sample in air at room temperature. The passivation layer, in combination with a thin film of the Nd-rich intergranular phases, if any, peculiarly appears to be non-magnetic compared with the main ferromagnetic $Nd_2Fe_{14}B$ phase. It keeps the ferromagnetic $Nd_2Fe_{14}B$ grains separated and thus inhibits mixing between the local magnetic lines of forces confined to them. As a result, they behave like ideal single-domain particles and therefore exhibit a reasonably improved H_{ci} value, without a significant decrease in the high J_r or the high saturation magnetization M_s which are useful for the high-energy-density magnets and related devices and components. The results are modelled and discussed with microstructures, magnetic properties, thermal stability and loss, if any, in the mass of the specimens during exposure to ambient atmosphere.

1. Introduction

The powders of $Nd_2Fe_{14}B$ of separated grains of critical single domain size, r_c, calculated to be 0.2 μm from domain structure analysis made by Durst and Kronmüller [1], are ideal for fabrication into anisotropic hard magnets and related devices and components of high energy densities. The coercivity, H_c, which is perhaps the most important parameter of these devices and which governs the high-energy product, $(BH)_{max}$, is a strong function of grain size (also morphology and surface structure of grain). It exhibits a maximum value of it on r_c-sized grains. The H_c value usually decreases over the smaller as well as the larger grains. The H_c in the large $r > r_c$ grains is governed by the so-called "the multidomain nucleation formalism" of coercivity. The grains of size $r > r_c$ have reversed magnetic domains, which are easily magnetized at relatively low applied magnetic fields along their easy axes of magnetization and exhibit a low H_c value [2]. Single-domain grains of considerably smaller sizes

Permanent address: Materials Science Centre, Indian Institute of Technology, Kharagpur, 721302, India.

0022–2461 © *1997 Chapman & Hall*

than the r_c value behave in a superparamagnetic manner and assume an $H_c = 0$ value on ideally superparamagnetic grains. This formalism has been successfully tested for hexagonal ferrites [2–5] and seems to be valid also for $R_2Fe_{14}B$ (where R is a rare-earth element) or similar other hard magnetic intermetallics [6].

It is feasible that r_c-sized separated single-domain $Nd_2Fe_{14}B$ grains are magnetically individually aligned with a single magnetization axis to form anisotropic magnets of optimal $(BH)_{max}$ on optimized values of remanence, J_r, and H_c. Such small $Nd_2Fe_{14}B$ grains are, of course, produced by rapid quenching [7–9] or powder metallurgical routes [9–12] followed by adequate thermal annealing, if necessary, but they stick together strongly in random orientations of their easy axes of magnetization and are impossible to align individually along a single easy axis (crystallographic *c* axis in the present example) of magnetization.

The cutting, crushing and grinding of the specimen necessary to separate the individual grains oxidize the grain surfaces and introduce several structural imperfections, which adversely lower the high H_c value considerably from 20–30 kOe (in the A-grade $Nd_2Fe_{14}B$ magnet) to a few kilo oersteds, or even lower, depending on the final grain size and on the amount of the imperfections. These imperfections destabilize the $Nd_2Fe_{14}B$ lattice and propagate oxidation as soon as the samples are exposed to air. As a consequence, the resultant powder is highly pyrophoric and readily oxidizes in an ambient atmosphere. The oxidation begins with Nd atoms which have a characteristically higher oxidation potential, ϕ, of -2.41 V, than iron ($\phi = -0.44$ V) or boron. The moisture (H_2O), if any, in the atmosphere activates the reaction by itself reacting with the highly reactive alloy surfaces through an internal production of high-energy and mobile nascent hydrogen:

$$\begin{aligned} &Nd + 3H_2O \rightarrow Nd(OH)_3 + 3H \\ &Nd + (2+\delta)H \rightarrow NdH_{2+\delta},\ \delta \leqslant 1 \\ &4NdH_2 + 5O_2 + 2H_2O \rightarrow 4Nd(OH)_3 \end{aligned} \qquad (1)$$

The $Nd(OH)_3$ slowly segregates and coats the associated $R_2Fe_{14}B$ grains at room temperature (the local temperature may be significantly higher) by the self-induced exothermic reactions (1). A coating of a few nanometres thickness, if immediately dried and stabilized by heating the specimen at 50–80 °C under a protective atmosphere, prevents further oxidation of the specimen in ambient atmosphere.

We explored this idea to synthesize substantially stabilized and oxidation-proof $R_2Fe_{14}B$ particles in air at room temperature by grinding the sample with a small addition of carbon, AlN or BN, and R_2O_3 (provided that the specimen does not contain a sufficient excess of R atoms over the $R_2Fe_{14}B$ composition) under hexane (with 5% water) followed by annealing the mixture in a pure N_2 gas at an elevated temperature. During annealing, some of these thermally rigid additives react with the $R_2Fe_{14}B$ grain surfaces and some of them stay in the grain boundaries, forming a thermally stabilized grain-surface passivation film rich in nitrides and carbides of involved species. Bogatin *et al.* [13] used a somewhat similar process to produce a stable powder of Nd–Fe–B ingots by milling the ingots (after cutting and crushing in sizes adequate for the milling) under water to the final particle size of the order of 10 μm. In this case, a reasonably large volume fraction of the refined particles is surface oxidized into a mixture of the non-magnetic oxides (or hydroxides or oxyhydroxides) of R or Fe and the soft magnetic α-Fe or Fe oxides. These soft magnetic impurities cause an unwanted asymmetric shape of the hysteresis loop of the sample with a dramatically lowered H_{ci} value [14], inadequate for practical applications. Nevertheless, milling in water is not advised to refine the size of particles of about 1 μm or smaller. Such small $R_2Fe_{14}B$ particles, without a protective grain-surface coating or any other protection against the expected oxidation, as mentioned above, become readily oxidized in water at room temperature and do not allow gas passivation and subsequent thermal treatments to stabilize the hard magnetic $R_2Fe_{14}B$ phase with a high value of H_{ci} and/or J_r.

The thin $R_2Fe_{14}B$ grain-surface passivation film (which is especially non-magnetic and which strongly adheres to the grains through chemical bonding with the oxidized R^{3+}-O^{2-} species in the grain surfaces) stabilized by the controlled grain-surface oxidation reactions with the above additives improves the stable H_{ci} value and in turn improves the high $(BH)_{max}$ value. It behaves as pinning barriers to the continuous motion of $R_2Fe_{14}B$ domain walls from grain to grain extending over several grains in an applied magnetic field. As proposed by Pinkerton and Fuerst [15], in the absence of the pinning barriers, the domain walls run continuously from grain to grain, forming an extended domain structure, which continues through several grains. This is one of the important reasons why R–Fe–B alloys having 5–28% excess R over the true $R_2Fe_{14}B$ composition usually exhibit high H_{ci} values. In this example, the excess R, which exists primarily as a non-magnetic intergranular phase with the ferromagnetic $R_2Fe_{14}B$ phase, behaves as pinning barriers. It therefore causes a high value of H_{ci} in combination with the characteristically large value of the magnetocrystalline anisotropy H_a of the primary $R_2Fe_{14}B$ phase, e.g., $H_a = 82.5$ kOe for $Nd_2Fe_{14}B$, as will be discussed later in section 3.1.1.

In the present article, we report the preliminary results of the synthesis of the refined $Nd_2Fe_{14}B$ powders together with the microstructure and the magnetic properties useful for permanent magnets and related devices. The loss, if any, in mass of the loose powder as well as when it is aligned and compacted into small magnets is systematically studied at selected intervals of time of exposures of the sample in open air in order to characterize the controlled oxidation, corrosion resistance and thermal stability of the sample in different shapes and forms of it in ambient atmosphere. Finally, the results are compared with parallel studies on similar powders obtained independently by a coreduction reaction (which was introduced many

years ago in 1971 by Cech [16, 17] for preparing $SmCo_5$-type alloys and was explored later by several other workers including our group [6, 14, 18, 19] for synthesis of Nd–Fe–B powders) of Nd_2O_3 and elemental iron and boron by calcium or calcium hydride at 900–1000 °C under vacuum or argon. This particular method directly yields a very fine powder of the alloy on a submicrometre scale of the grain or particle size. The pure alloy powder is recovered and stabilized as a result of grain-surface passivation by washing away the byproducts in water and then immediately drying the recovered sample in vacuum at room temperature.

2. Synthesis and measurements

2.1. Rapid quenching

Several compositions of Nd–Fe–B alloys were synthesized by two different methods: firstly rapid quenching; secondly co-reduction reaction of appropriate Nd_2O_3, Fe and B mixtures by calcium metal or calcium hydride. Those which exhibited outstanding magnetic properties for high-energy-density permanent magnets are listed in Table I.

In the first method, a total of 15 g of ingots of Nd, Fe and B metals was melt spun on the surface of a rapidly spinning copper wheel under pure argon using quartz tubes with orifice diameters of 0.31 mm and 0.52 mm, respectively. This yielded thin ribbons of length 50 mm, width 2 mm and thickness 15–30 μm. Magnetic properties, especially the intrinsic coercivity, H_{ci}, of these ribbons were noticed to be highly sensitive to the substrate velocity, v_s. A maximum H_{ci} value, irrespective of composition, appeared at a typical $v_s = 16\ m\ s^{-1}$ at an orifice diameter of 0.52 mm, as shown in Fig. 1.

2.2. Grain size and grain-surface refinements

The ribbons were cut, crushed and milled into 1–5 μm flakes under H_2 gas using an attritor-type machine. During the milling, the hydrogen diffuses to the interstitial sites in the alloy embrittling it, allowing easy powdering. These hydrided flakes were mixed with a total of 5 wt % Nd_2O_3, carbon and AlN or BN (in 1:2:2 ratio) and then were finely milled to about 1 μm with steel balls under hexane using 5% water. The water wets and reacts with the fresh alloy grain surfaces and allows the additives to adhere and uniformly coat the grains through chemical bonding with the oxygen atoms in the oxide species at the grain surfaces. The coating (passivation) layer is stabilized by partial oxidation and becomes thermally rigid and further oxidation proof on annealing for 1–2 h at 300 °C followed by about 30 min at higher temperatures of 600–700 °C under N_2 gas at approximately 1 bar. This results in a reasonably stable refined powder of about 1 μm average grain size.

A further refinement of the grain size is possible by a thermal decomposition and recrystallization of the H-destabilized $Nd_2Fe_{14}BH_x$, $x \leqslant 5$, hydrides at an elevated temperature. The anhydride $Nd_2Fe_{14}B$ particles absorb hydrogen on heating in H_2 gas at approximately 1 bar and 150–200 °C and form $Nd_2Fe_{14}BH_x$, $x \leqslant 5$, hydrides, which are stable at room temperature in an inert-gas atmosphere. On a slow reheating (at a heating rate of about 5 °C min^{-1}) over 250–600 °C in controlled atmosphere in N_2 gas at approximately 1 bar, in a closed and confined volume, most of the H atoms slowly desorb reversibly without decomposition of the $Nd_2Fe_{14}B$ crystal lattice. Around 600 °C, the interstitial H atoms, which are still present in a significant fraction, become highly mobile, whereas other atoms in the lattice are relatively immobile, and those are therefore released by fragmentation of the alloy into extremely refined (amorphous or nanocrystalline) particles. H absorption or H-induced grain refinement in $R_2Fe_{14}B$ is not a new observation [20–23], but no one has used it so far in combination with N_2 gas, which is very helpful to obtain the refined particles and to pump off the unwanted hydrogen (as NH_3 gas) in the final recrystallization $R_2Fe_{14}B$ reactions. This powder still contains some hydrogen, which is removed only by continuously pumping it off with N_2 gas above 600 °C, through an efficient vacuum pump. The resultant material recrystallizes at 700–800 °C under a dynamic vacuum and yields a high-H_{ci} powder of reasonably separated $Nd_2Fe_{14}B$ grains. These grains are highly susceptible to oxygen and catch fire in air, but it is possible to stabilize these grains by grain-surface passivation and then they could be stored in argon or

TABLE I Saturation magnetization, M_s, intrinsic coercivity, H_{ci}, remanence, J_r and Curie temperature, T_C, of optimally quenched Nd–Fe–B alloys

Composition	M_s (emu g^{-1})	H_{ci} (kOe)	J_r (kG)	T_C (°C)
$Nd_{11.8}Fe_{82.3}B_{5.9}$	165	5	8.5	312
$Nd_{14.5}Fe_{80.0}B_{5.5}$	163	25	7.5	—
$Nd_{24.5}Fe_{70.0}B_{5.5}$	120	28.3	5.0	—
$Nd_{12.2}Fe_{76.9}Co_{5.5}B_{5.4}$	160	15.0	8.2	359
$Nd_{15.5}Fe_{63.0}Co_{16.0}B_{5.5}$	155	18.0	7.8	470

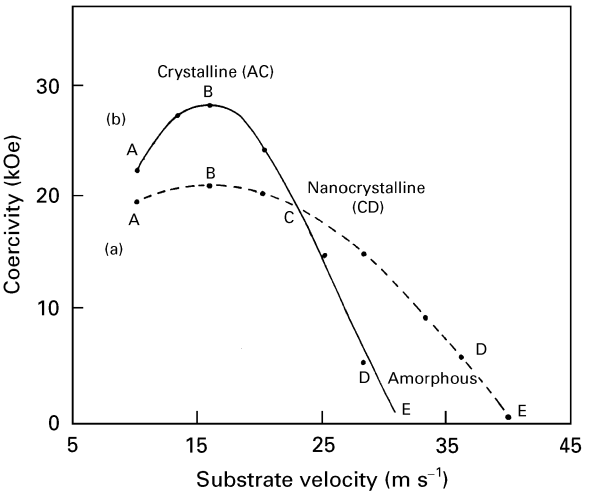

Figure 1 Intrinsic coercivity H_{ci} versus melt spinner substrate velocity v_s for $Nd_{24.5}Fe_{70.0}B_{5.5}$ ribbons prepared at orifice diameters of (a) 0.31 mm and (b) 0.52 mm. A maximum $H_{ci} = 28.3$ kOe appeared for single domain grains (0.15 μm size) in (b) at $v_s = 16\ m\ s^{-1}$.

acetone or similar other non-reactive hydrocarbon liquids.

2.3. Chemical reduction reactions

The elemental iron (or cobalt), boron (or ferroboron) and Nd_2O_3 were thoroughly mixed together by grinding under anhydrous acetone and then the resultant material was co-reduced by calcium granules (about 1 mm size) at 900–1000 °C in a pure argon atmosphere. At this temperature, there is an uptake of oxygen by the calcium from Nd_2O_3 to yield Nd metal which simultaneously reacts with Fe and B in the mixture and forms separated $Nd_2Fe_{14}B$ grains coated in CaO byproduct. A small (10 wt %) addition of $CaCl_2$ and NaCl helps the homogeneous reaction to form uniformly sized $Nd_2Fe_{14}B$ particles by conducting exchange of the local heat produced in the exothermic reaction. The reacted mixture, when cooled to room temperature, was washed in fresh water and the pure alloy was recovered and immediately dried under vacuum at room temperature or slightly higher. This results in a finely divided loose alloy powder, with a grain size of about 1 μm, which is peculiarly stable owing to the grain-surface passivation and can be stored in dry air at room temperature.

2.4. Measurements

The formation of crystalline $Nd_2Fe_{14}B$ phase or precipitation of any secondary phase in the above reactions were analysed using X-ray diffractometry (studied on a Siemens Kristalloflex diffractometer with filtered Cu Kα radiation). Microstructures of the selected specimens were studied with a scanning electron microscope and a transmission electron microscope. Elemental analysis was carried out with an X-ray detector in conjunction with the scanning electron microscope.

The magnetic properties were measured on a vibrating-sample magnetometer (VSM) having a provision for automatic sample centring controlled through a computer data aquisition with a magnetic field as high as 80 kOe, unless otherwise stated. The ferromagnetic-to-paramagnetic transition or any other magnetic transitions in $Nd_2Fe_{14}B$ were studied by measuring thermomagnetograms of the specimens at fixed magnetic fields of 1–2 kOe with a similar VSM in conjunction with a high-temperature oven assembly to control and vary the temperature in the range 25–600 °C. The sample temperature was monitored with a Pt–Rh thermocouple. Low temperatures between 295 and 4.2 K were achieved and varied through liquid helium as the coolant. These were monitored by a thermocouple of Au (Fe) versus normal silver.

3. Results and discussion

3.1. High coercivity in rapidly quenched fine microstructures

3.1.1. Dependence of H_{ci} on grain size and intergranular phases

The H_{ci} versus v_s plot, which exhibits a maximum at a particular $v_s = 16\ m\ s^{-1}$ in Fig. 1, supports the multidomain nucleation formalism of H_{ci} in this example. A maximum $H_{ci} = 28.3$ kOe value thus occurs in an optimally set-up fine microstructure of $r_c \approx 0.15$ μm single-domain grains of $Nd_2Fe_{14}B$ at point B (Fig. 1). The present value of $r_c \approx 0.15$ μm is slightly smaller than the value of 0.2 μm proposed by Durst and Kronmüller [1] from the domain structure analysis. The X-ray diffractogram of this sample (Fig. 2) exhibits only the characteristic lines of $Nd_2Fe_{14}B$. According to the equilibrium phase diagram [9], several minority phases, especially $NdFe_4B_4$, Nd_2FeB_3 and Nd_2Fe_{17} or its Nd-rich $L \rightarrow Nd_2Fe_{17}$ eutectic phase, are expected, but none was detected in the X-ray diffractogram. They most probably coexist in amorphous or fine nanocrystalline forms uniformly dispersed in the grain boundaries and therefore do not show up in conventional diffractometry. Electron micrographs of these specimens do show some amorphous particles. For example, Fig. 3 shows a typical transmission electron micrograph of a high-H_{ci} crystalline Nd–Fe–B powder. The $Nd_2Fe_{14}B$ crystal particles of characteristically sharp edges exhibit well-defined diffraction patterns of ordered arrays of reflection points (Fig. 3b). These are accompanied by further smaller grains regularly distributed in the grain boundaries, reflecting the diffractograms of diffuse rings (Fig. 3c) characteristic of amorphous materials. Yin *et al.* [24] studied electron microscopy of similar Nd–Fe–B alloys and confirmed that $Nd_2Fe_{14}B$ crystallites coexist with $NdFe_4B_4$ and Nd-rich phases. They found that the $NdFe_4B_4$ phase had an incommensurate tetragonal structure with stacking faults in the Fe sites. The Nd-rich phase had a face-centred cubic ($a = 5.2$ Å) + complex body-centred cubic ($a = 10.4$ Å) structure. This is the case for a well-recrystallized Nd–Fe–B alloy which, as expected, does not exhibit a high H_{ci} value. We studied systematically the microstructure and magnetic properties of several types of samples and found that a high H_{ci} value always results for fine $Nd_2Fe_{14}B$ grains accompanied with a regular distribution of a secondary phase(s) of no defined crystalline structure in the grain boundaries.

Half-bandwidths $\Delta(2\theta_{1/2})$ in the $Nd_2Fe_{14}B$ characteristic peaks vary with the grains size following the Debye–Scherrer relation

$$D = \frac{\lambda}{\Delta(2\theta_{1/2})\cos\theta} \qquad (2)$$

where D is the average diameter of the grain and λ is the wavelength of the X-ray beam used to monitor the diffraction patterns. Some 20 representative lines recorded at an expanded scale in the range 20–50 ° of 2θ have been fitted to Voigt functions from which the integral bandwidth $\beta = \Delta(2\theta_{1/2})$ is estimated following the results of Langford [25]. It allowed calculation of D values, using different values of β and cos θ for different peaks in Equation 2, whose averaged value represents the average grain size. We explored the results with three representative specimens of 1.0, 0.5 and 0.15 μm grain size. In all cases, the variation in $\Delta(2\theta_{1/2})$ strictly follows the variation in the grain size within the experimental errors. An average value of

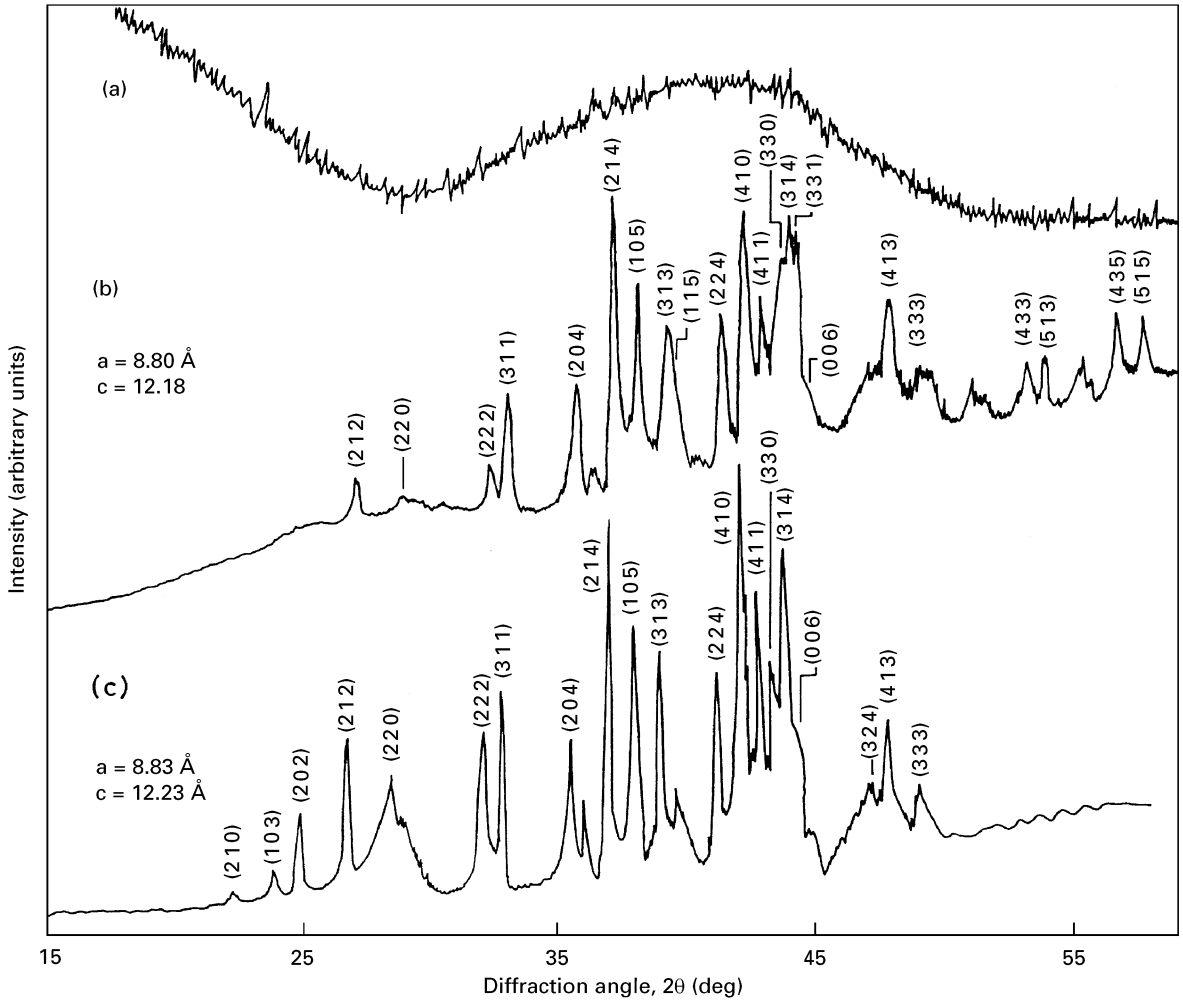

Figure 2 X-ray diffractograms of $Nd_{14.5}Fe_{80.0}B_{5.5}$ ribbons: (a) amorphous or nanocrystalline, (b) crystalline, 0.15 μm average grain size, (c) crystalline, 1 μm average grain size.

$D = 0.12$ μm was thus found as against 0.15 μm observed directly from the electron micrographs.

The v_s controls the precipitation and growth of $Nd_2Fe_{14}B$ grains during melt spinning of the ribbons. As a result, very fine particles (or domains) due to nanocrystalline or amorphous $Nd_2Fe_{14}B$, characterized by broad X-ray diffraction peaks (Fig. 2b) or broad X-ray diffraction haloes (Fig. 2c) or diffuse rings in the electron diffractogram (similar to that shown in Fig. 3c), appeared at high v_s (above 16 m s^{-1}) in regions CD and DE in Fig. 1. Those have progressively decreasing H_{ci} values from over a few kilo oersteds to almost zero in the progressively growing superparamagnetic nature in the increasingly finer $r < r_c$ grains.

According to classical nucleation theory, the activation energy threshold (the free-energy change) ΔF in the formation of a critical nucleus is written as

$$\Delta F = \frac{16\pi\sigma^3}{3(\Delta G_v)^2} f(\Theta) \tag{3}$$

where σ is the interfacial energy of the solid–liquid interface, $f(\Theta)$ is the catalytic potency factor for hetrogeneous nucleation, which depends on the wetting angle Θ [26], and ΔG_v is the free-energy change per unit volume involving the precipitation of a particular phase within the system. This model reveals the critical size r^* of the associated crystals (having the maximum free energy) given by the relation

$$r^* = \frac{2\sigma}{\Delta G_v} \tag{4}$$

In most cases, the value of r^* comes within the range of a few nanometres only, i.e., much smaller than r_c. These so-called "nanocrystals" have a characteristically high surface energy ($4\pi r^2\sigma$) and form a metastable phase of the given material. Such small crystals of ferromagnetic materials of even a very high magnetocrystalline anisotropy, H_a, such as in $Nd_2Fe_{14}B$, behave as superparamagnetic particles by predominant thermal energy over their anisotropy energy, E_a. As a result, they assume a thermally random distribution of magnetic spins with no exchange interactions. Our results on H_{ci} of rapidly quenched alloys, which present rapidly decreasing H_{ci} values between points C and E in Fig. 1 with decreasing size of the crystals in the range 100–10 nm, support this model. Davies *et al.* [27] reported high H_{ci} values in the so-called "$Nd_2Fe_{14}B$ nanocrystals" but, of course, these were

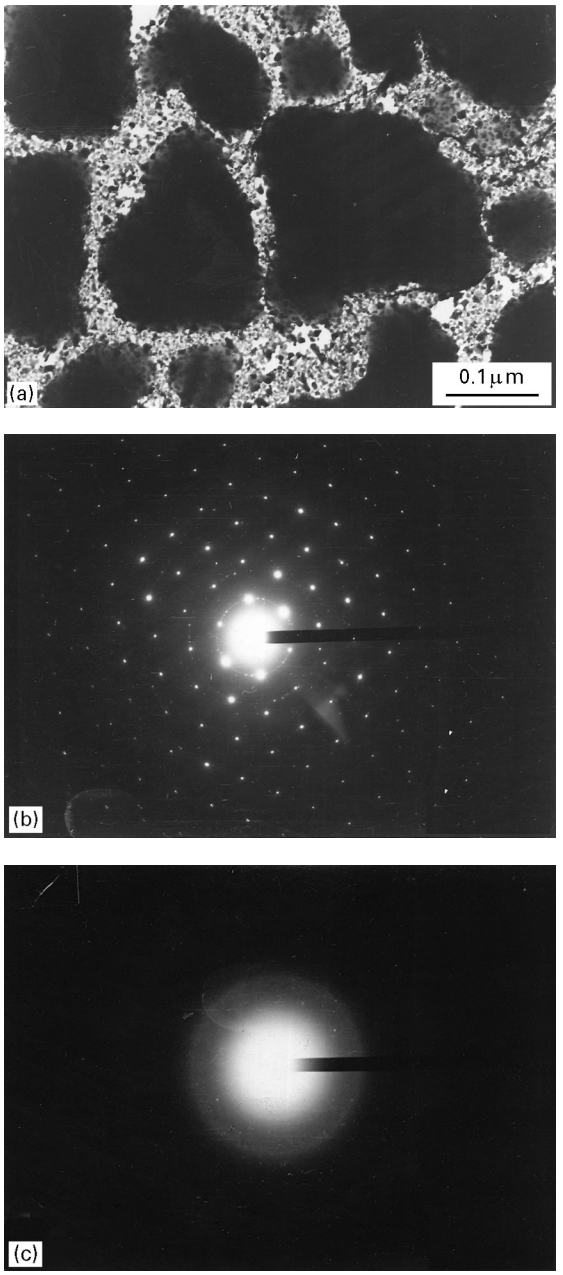

Figure 3 (a) Transmission electron micrograph of a high coercivity $Nd_{14.5}Fe_{80.0}B_{5.5}$ alloy, (b) diffractogram recorded from the well-defined grains, in (a), and (c) diffractogram recorded from the associated grain-boundary phases.

far larger than an order of magnitude larger than r^* in size and, in fact, to call them nanocrystals is not accurate.

Exact stoichiometry of the hard ferromagnetic phase in the ternary Nd–Fe–B alloys is not known but it is very close to $Nd_2Fe_{14}B$. This means that the typical alloys which exhibit the high H_{ci} values always correspond to considerable amounts of a secondary phase (s). For example, a $Nd_{24.5}Fe_{70.0}B_{5.5}$ alloy, which exhibits the highest $H_{ci} \approx 28.3$ kOe value, contains at least 27.9 wt % excess Nd in the secondary (amorphous or nanocrystalline) phase of probably a total composition of the ternary eutectic $Nd_{67}Fe_{26}B_7$, as proposed by Matsuura *et al.* [28]. In this approximation, the present alloy contains another phase than $Nd_2Fe_{14}B$ which has x equal to at least 23.5% to balance the total alloy composition, i.e.,

$$\Phi(R) = (1 - x)\Phi(F) + x\Phi(I) \quad (5)$$

where $\Theta(R)$, $\Phi(F)$ and $\Phi(I)$ refer to the formula weights of the resultant alloy, ferromagnetic ($R_2Fe_{14}B$) phase and intergranular phase (of fractional ratio x), respectively. Whatever the mechanism of their formation in equilibrium with the main phase, these so-called "intergranular phases" coexist with the ferromagnetic $Nd_2Fe_{14}B$ phase and contribute apparently no positive magnetic moment (which is evident from the decrease in total M_s of the specimen) to the total M_s of the resultant material but support the magnetic hardening of the isolated single-domain $Nd_2Fe_{14}B$ grains, as discussed below.

3.1.2. Multidomain nucleation formalism of H_{ci} in Nd–Fe–B alloys

Note that the basic principles of magnetization in $R_2Fe_{14}B$ intermetallics are essentially the same as in hexagonal ferrites or other hard magnetic materials, and hence to propose an altogether different mechanism [1, 15] of H_{ci} especially for these particular intermetallics is not logical. Deliberately added non-magnetic intergranular inclusions in these alloys just supports the magnetic hardening of isolated r_c-sized single-domain $Nd_2Fe_{14}B$ grains of characteristically high $H_a = 82.5$ kOe [22]. It is this high H_a value which primarily results in the high H_{ci} value in these alloys on especially fine-grained microstructures.

Thus, in the most general case, H_{ci} for an assembly of isolated single-domain grains can be best described following the Stoner–Wohlfarth [29] theory. Taking into account the dynamic effects of the non-magnetic (i.e., diamagnetic or weakly paramagnetic, as will be discussed later) intergranular inclusions, α, to allow independent motion of domain walls in the isolated ferromagnetic $Nd_2Fe_{14}B$ grains it predicts that

$$H_{ci} = P\frac{\alpha}{\beta}(H_a - H_b) \quad (6)$$

where P is the geometrical parameter, which assumes an empirical value of 0.48 for thin platelets of hexagonal ferrites [30–33], and β defines the figure of merit of single-domain grains in the ensemble. The value of the shape anisotropy, H_b, varies according to morphology of the grains, i.e., $H_b = 0$ for perfectly spherical, $2\pi M_s$ for acicular and $4\pi M_s$ for platelet shapes. Obviously, the former two shapes exhibit the lowest H_b and the highest possible H_{ci} value but those unusual shapes were never achieved in these examples.

Equation (6) reveals an H_{ci} value as high as 66.3 kOe for absolute $\alpha_0 = P\alpha = 1$, and $\beta = 1$ values, with $H_a = 82.5$ kOe and $H_b = 4\pi M_s\rho = 16.2$ kOe (assuming that $\rho = 7.66\ g\,cm^{-3}$, the bulk density, and $M_s = 168\ emu\,g^{-1}$ as in $Nd_2Fe_{14}B$ single crystals [34–36]), for perfectly non-interacting isolated r_c-sized single-domain ferromagnetic $Nd_2Fe_{14}B$ grains. This is the optimum value which can be achieved in this alloy in these ideal conditions at room temperature. Thus an H_{ci} value as high as 28.3 kOe found experimentally

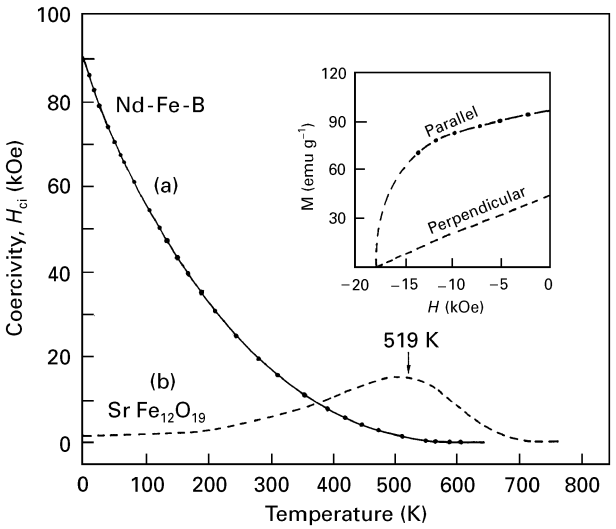

Figure 4 Variation in H_{ci} with temperature in die-upset (a) $Nd_{13.9}Fe_{80.6}B_{5.5}$ and (b) $SrFe_{12}O_{19}$ magnets. The inset shows the room-temperature second-quadrant demagnetization curves measured in parallel and perpendicular orientations to the press direction for the sample (a). The $H_{ci} \approx 17.12$ kOe value apparently does not change with orientation of the sample. Sample (b) had a small 10% substitution of Fe^{3+} by Al^{3+} in order to obtain an improved H_{ci}, which assumes its maximum value at $T_p \approx 519$ K in critical single-domain grains.

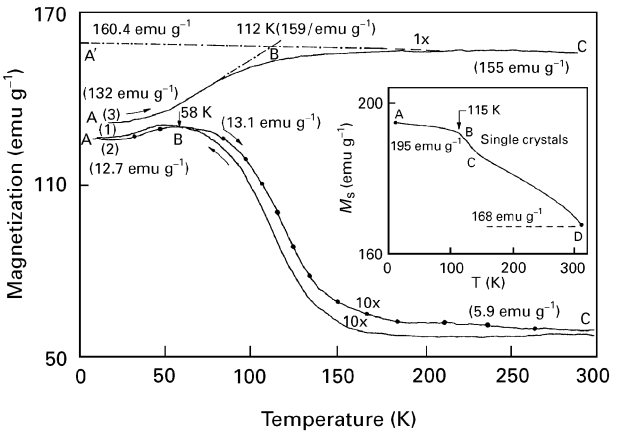

Figure 5 Thermomagnetograms of crystalline $Nd_{15.5}Fe_{63.0}Co_{16.0}B_{5.5}$ recorded at (1) 10 kOe, (2) 10 kOe and (3) 80 kOe. Curve (1) is measured in the cooling cycle while curves (2) and (3) are measured in the heating cycle. The scale bar on the y-axis applies to curve (3). It should be divided by a factor of 10 in curves (1) and (2). In the inset is shown an M_s versus T plot for $Nd_2Fe_{14}B$ single crystals.

in $Nd_{24.5}Fe_{70.0}B_{5.5}$ alloy at room temperature is considerably lower than this theoretically expected value. Moreover, the experimental H_{ci} value is found to be monotonically enhanced on cooling the specimen below room temperature and it provides a fairly good agreement with the theoretical value in ideal conditions for $\alpha_0 = 1$ and $\beta = 1$ satisfied at 4.2 K. The enhanced values of H_{ci} and H_a at 4.2 K were not possible to measure exactly in the limited magnetic fields used in these experiments. Fig. 4 portrays an H_{ci} versus T plot for a similar alloy of slightly lower H_{ci} value in the measurable range, i.e., $H_{ci} \approx$ 17.12 kOe at room temperature and $H_{ci} \approx 87$ kOe at 4.2 K.

The $Nd_{24.5}Fe_{70.0}B_{5.5}$ alloy contains a total of 27.9 wt % excess Nd (over the true $Nd_2Fe_{14}B$ composition), which forms the intergranular phase, which eventually behaves as non-magnetic compared with the ferromagnetic $Nd_2Fe_{14}B$. It modifies the exchange interactions, J_{FG}, which are normally neglected (but appear to be especially important in this particular example), between the ferromagnetic $Nd_2Fe_{14}B$ grains by inhibiting mixing of local magnetic lines of forces over isolated $Nd_2Fe_{14}B$ grains. The modified J_{FG} on the modified $Nd_2Fe_{14}B$ grain surfaces eventually led to a modified decrease in the total M_s at low temperatures, effectively below 200 °C, with the onset temperature T_{md} at 112 K (determined by the intersection of two straight lines in the thermomagnetogram in Fig. 5). The physical significance of T_{md} is that it defines a critical temperature below which the total M_s rapidly decreases on further decreasing the temperature, basically governed by the spin reorientation transitions of the atomic magnetic moments of Fe and Nd atoms in the $Nd_2Fe_{14}B$ lattice. At $T \geqslant T_{md}$, the magnetic moments of both Fe and Nd atoms are collinear with the crystallographic c axis in the $Nd_2Fe_{14}B$ crystal lattice, but they undergo spin reorientations at a particular temperature, T_{SR} (here $T_{SR} \approx T_{md}$), making a resultant angle θ_c with the c axis, which monotonically increases on further decreasing the temperature to $T = 0$ [9]. The $Nd_2Fe_{14}B$ single crystals, which do not have any intergranular phase, do not exhibit such pronounced effects of the spin reorientations on the total M_s in this region (cf., the thermogram in the inset in Fig. 5). Thus the total M_s of this binary magnetic (ferromagnetic and non-magnetic or weakly paramagnetic) phase material can be expressed by

$$M_s = (1 - x)M_s(\mathrm{F})\cos\theta + xM(\mathrm{I}) \qquad (7)$$

where x is the fractional ratio of the intergranular phase of magnetic moment $M(\mathrm{I})$ and $M_s(\mathrm{F})$ is the magnetic moment of the $Nd_2Fe_{14}B$ primary ferromagnetic phase, which is apparently modified by a factor of $\cos\theta$, in the $T \leqslant T_{md}$ region, by the spin reorientation transitions.

Equation 7 yields the value of $M(\mathrm{I})$ given by

$$M(\mathrm{I}) = -\frac{(1 - x)M_s(\mathrm{F})\cos\theta - M_s}{x}$$

or

$$M(\mathrm{I}) = M_s(\mathrm{F})\cos\theta - \frac{\Delta M_{FS}}{x} \qquad (8)$$

where $\Delta M_{FS} = M_s(\mathrm{F})\cos\theta - M_s$ is the apparent contribution of the intergranular phase to the total magnetization of the specimen. If we presume that $M(\mathrm{I}) \approx 0$ for the time being, our experimental data in Fig. 5 yield

$$M_s(\mathrm{F})\cos\theta = \frac{132}{1 - x}\ \mathrm{emu\ g^{-1}} \qquad (9)$$

and

$$M_s(\mathrm{F}) = \frac{160.4}{1 - x}\ \mathrm{emu\ g^{-1}} \qquad (10)$$

TABLE II Analysis of coercivity H_{ci} with the structural factors, P, α, α_0 and β, in Nd-rich $Nd_2Fe_{14}B$ alloys, with magnetocrystalline anisotropy $H_a = 82.5$ kOe and shape anisotropy $H_b = 16.2$ kOe

Sample [a]	Parameters				Coercivity H_{ci} (kOe)	
	P	α	α_0	β	Observed	Calculated
(1) $Nd_{11.8}Fe_{82.3}B_{5.9}$	0.48	0.18	0.086	1.12	5.0	5.1
(2) $Nd_{14.5}Fe_{80.0}B_{5.5}$	0.48	0.88	0.422	1.12	25.0	25.0
(3) $Nd_{24.5}Fe_{70.0}B_{5.5}$	0.48	1.00	0.480	1.12	28.3	28.4

[a] Samples (2) and (3) contain totals of 6.7 and 27.9 wt % excess neodymium, respectively, with respect to an almost $Nd_2Fe_{14}B$ composition in sample (1).

obtained at 4.2 K by extrapolating the straight line CB to point A′. Division of Equation 9 by Equation 10 implies the critical value of $\cos\theta^* = 0.82$, or $\theta^* = 34.62^\circ$, which matches fairly well the value of the resultant tilting angle (of the magnetic moments of Fe and Nd atoms from the crystallographic c axis in the $Nd_2Fe_{14}B$ lattice) $\theta_c = 30^\circ$, obtained for single $Nd_2Fe_{14}B$ crystals by magnetization measurements and torque measurements at this temperature [37].

Substituting the observed values of $M_s(F) = 195\ \text{emu g}^{-1}$ (for the single crystals) and ΔM_{FS} $(= 195\cos\theta_c - 132) = 28.47\ \text{emu g}^{-1}$, at 4.2 K, in Equation 8, we get

$$M(I) = 160.47 - \frac{28.47}{x}\ \text{emu g}^{-1} \qquad (11)$$

at 4.2 K. It predicts a value of $M(I) \approx 0$ (at 4.2 K) at $x \approx 0.177$, and a positive value at a reasonably larger x value, which is appropriate in this example. It is confirmed that the intergranular phase is certainly a non-magnetic phase. Note that every material has a more or less diamagnetic character, and that operates by modified orbital motion of involved electrons in an applied magnetic field. The single-domain $Nd_2Fe_{14}B$ grains, with the grain surfaces or grain boundaries modified by the non-magnetic surface coatings or by the presumed non-magnetic intergranular phases, probably have an enhanced effective diamagnetic contribution at low temperatures and that helps to isolate (repel) strongly the local magnetic lines of forces of adjacent ferromagnetic grains to concentrating over the individual grains. Whatever the real mechanism, it obviously improves α and thus qualitatively accounts for the monotonically increasing H_{ci} value observed with decreasing temperature between 600 and 4.2 K in Fig. 4.

The magnetic interaction between the two phases depends on firstly the spontaneous magnetization of the ferromagnetic phase, secondly the field applied to magnetize the specimen and thirdly the temperature during the measurement. At a given temperature $T \leqslant T_{md}$, where the phase concerned is strongly effective, the interaction indeed varies with applied field and the specimen responds differently at different magnetic fields. At effectively low fields of 10 kOe or lower, it behaves as a soft magnetic material, with a reasonably low H_{ci} value, a low magnetization and the magnetization peaks (cf., curves 1 and 2 in Fig. 5) between 4.2 and 150 K. The position of the peak varies according to the competitive interactions between the internal fields in the specimen developed on applied fields during the measurement. This particular signal does not appear in single crystals or powders of pure $Nd_2Fe_{14}B$ synthesized by co-reduction of Nd_2O_3, Fe and B by calcium. In this case, in which the specimen does not have any intergranular phase (except a passivation of grain surfaces), the M versus T thermomagnetogram exhibits only a small peak at $T \approx 125$ K, in the spin reorientation transition [9, 35], followed by a regular increase in M with decreasing T up to 4.2 K. Also the saturation magnetization M_s regularly increases with decreasing T between 300 and 4.2 K, with a slightly changed slope at T_{SR} (cf., the thermomagnetogram in Fig. 5).

The alternating-current susceptibility of $Nd_2Fe_{14}B$ powder [38] or single crystals [39] exhibits weak magnetic orderings in this region in extremely low magnetic fields of the order of 1 Oe or lower. This small magnetic field hardly deals with about 0.01% of total magnetic spins in the specimen, and those, of course, do not contribute to its hard magnetic properties. These should not be confused with the rather strong ferromagnetic interactions that we discussed above.

It is true that the specimens in question always have significant amounts of superparamagnetic $Nd_2Fe_{14}B$ grains and these satisfy a higher value of β than 1 for r_c-sized single-domain grains. These superparamagnetic grains take part in magnetization, especially at high magnetic fields, of the total specimen and influence the final H_{ci} value. Thus an empirical value of $\beta = 1.12$, assuming the other parameters to be constant, in Equation 6, yields $H_{ci} = 28.4$ kOe for a typical $Nd_{24.5}Fe_{70.0}B_{5.5}$ alloy, in agreement with the observed 28.3 kOe value. Other samples listed in Table II have the same value of $\beta = 1.12$ but reasonably different values of α, solely governed by the amounts of the non-magnetic materials in the $Nd_2Fe_{14}B$ grain-surface layers.

3.2. Multidomain nucleation formalism of H_{ci} in hexagonal ferrites

The same multidomain nucleation formalism of H_{ci} as in $R_2Fe_{14}B$ intermetallics holds good in the hexagonal ferrites as well. Table III compares the results obtained for the representative samples. As expected, the single-domain grains of the ferrites require a relatively thin non-magnetic coating to have a similarly improved α value according to their lower

TABLE III Coercivity, H_{ci}, and structural parameters, P, α, α_0 and β, in $SrFe_{12}O_{19}$ ceramic powders with presumed magnetocrystalline anisotropy $H_a = 16.8$ kOe and shape anisotropy $H_b = 4.68$ kOe

Sample	Parameters				M_s (emu g^{-1})	H_{ci} (kOe)	
	P	α	α_0	β		Observed	Calculated
$SrFe_{12}O_{19}$	0.48	0.60	0.288	1	71	3.50	3.49
$Sr_{0.9}Ca_{0.1}Fe_{12}O_{19}$	0.48	0.80	0.384	1	75	4.70	4.65
$SrFe_{12}O_{19}$ coated by 1 wt % Al_2O_3 at 1000 °C for 3 h	0.48	1.00	0.480	1	70	5.80	5.81

TABLE IV Magnetic properties of refined Nd–Fe–B powders by grinding with a total of 5 wt % additive of Nd_2O_3, carbon and AlN (or BN) and then annealing the resultant material for 30 min at 700 °C in N_2 gas at 1 bar

Alloy	M_s (emu g^{-1})	H_{ci} (kOe)	J_r (kG)	T_C (°C)
$Nd_{11.8}Fe_{82.3}B_{5.9}$	159	4.2	10.5	375
$Nd_{13.9}Fe_{80.6}B_{5.5}$	158	18.0	10.0	—
$Nd_{24.5}Fe_{70.0}B_{5.5}$	117	22.0	7.0	—
$Nd_{12.2}Fe_{76.9}Co_{5.5}B_{5.4}$	157	10.0	9.0	—
$Nd_{14.0}Fe_{63.6}Co_{16.9}B_{5.5}$	153	15.9	7.7	490
$Nd_{15.5}Fe_{63.0}Co_{16.0}B_{5.5}$	152	17.1	8.1	—

$M_s \approx 71$ emu g^{-1} (compared with 168 emu g^{-1} for $Nd_2Fe_{14}B$) at room temperature. We found that Al_2O_3 easily coats $SrFe_{12}O_{19}$ hexagonal ferrite grains by milling with the requisite amount (about 5 wt %) of $Al(NO_3)_3 \cdot 9H_2O$ under alcohol or water and then annealing at 1000 °C for 3 h. At this temperature, which is insufficient to cause any grain growth of fine grains of 0.5 μm or larger, the Al_2O_3 (obtained by thermal decomposition of the nitrate) segregates and coats the individual $SrFe_{12}O_{19}$ grains with optimized grain-surface energy by removing the strain and other structural imperfections added during the milling. It led to a dramatic improvement in H_{ci} from 3.50 kOe to 5.80 kOe at room temperature.

3.3. Finishing of stable $Nd_2Fe_{14}B$ powders

A technical disadvantage with the optimally quenched Nd–Fe–B ribbons is that they slowly oxidize and lose their high H_{ci} and M_s values in ambient atmosphere. For example, figs 6 and 7 demonstrate the loss in H_{ci} and M_s measured as functions of exposure of typical samples in an ambient atmosphere. A $Nd_{11.8}Fe_{82.3}B_{5.9}$ ribbon (i.e., of exact $Nd_2Fe_{14}B$ composition) exhibits a maximum M_s loss of 42% within the first 100 h exposure in Fig. 7a. Use of approximately 27.9 wt % excess Nd (over $Nd_2Fe_{14}B$) in another ribbon of $Nd_{24.5}Fe_{70.0}B_{5.5}$ composition markedly balanced the M_s loss at 5 wt % but it adversely lowered M_s ($= 120$ emu g^{-1}). We tried several combinations of Nd and Fe and came to the conclusion that the compositions having 5–10 wt % excess Nd yield the best optimized result of $H_{ci} = 20$–25 kOe and $M_s = 150$–163 emu g^{-1} (as against $M_s = 165$ emu g^{-1} and $H_{ci} \approx 5$ kOe for pure $Nd_2Fe_{14}B$ in Table I).

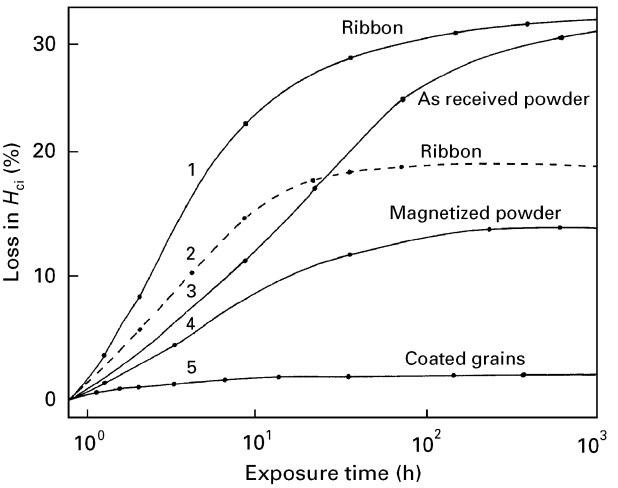

Figure 6 Loss in H_{ci} in optimally quenched $Nd_{15.5}Fe_{63.0}Co_{16.0}B_{5.5}$ ribbons (grain size, 0.14 μm) (curves 1 and 2) and the powdered ribbons (grain size, about 1 μm) (curves 3–5) during exposure to the laboratory atmosphere. The loss is considerably reduced on magnetizing and compacting the powder (curve 4), especially using the grain-surface passivation (curve 5) by carbon and other additives.

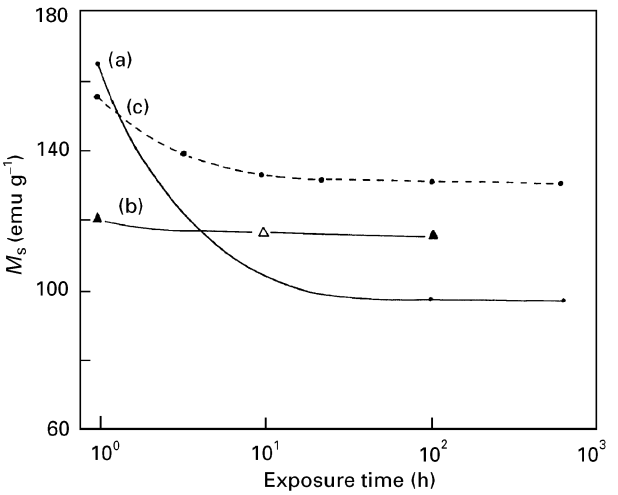

Figure 7 Loss in M_s of optimally quenched (a) $Nd_{11.8}Fe_{82.3}B_{5.9}$, (b) $Nd_{24.5}Fe_{70.0}B_{5.5}$ and (c) $Nd_{15.5}Fe_{63.0}Co_{16.0}B_{5.5}$ ribbons during exposure to the laboratory atmosphere.

A partial $Nd_2Fe_{14-x}Co_xB$ substitution of Fe by Co is often used to boost the modest $T_C \approx 315$ °C of primary $Nd_2Fe_{14}B$ phase in these alloys. The Co increases T_C about 70 °C per 0.1 increment in x [40]. It also improves H_{ci}, by as much as 60%, for very low $x = 0.03$–0.06 substitutions without decreasing M_s or

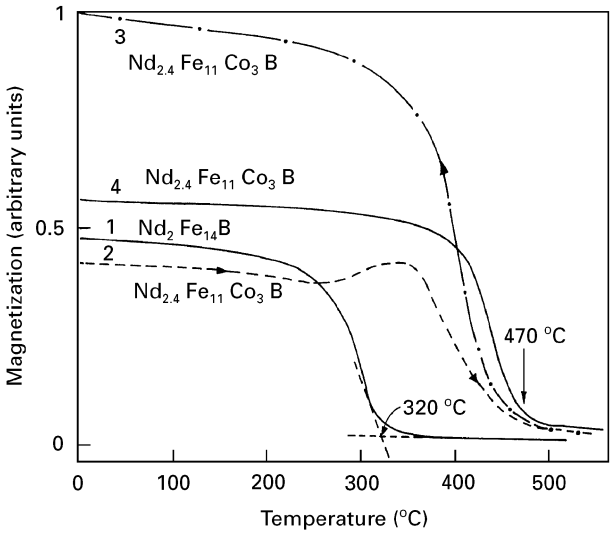

Figure 8 Thermomagnetograms of $Nd_2Fe_{14}B$ single crystals (curve 1) and $Nd_{15.5}Fe_{63.0}Co_{16.0}B_{5.5}$ ribbons (curves 2–4) measured under a magnetic field of 2 kOe. Curves 2 and 3 are measured in heating and cooling, respectively. T_C is significantly improved from 450 to 470 °C in curve 4 on grain-surface treatment by heating the powder with 1 wt % carbon and AlN at 400–500 °C under N_2 gas.

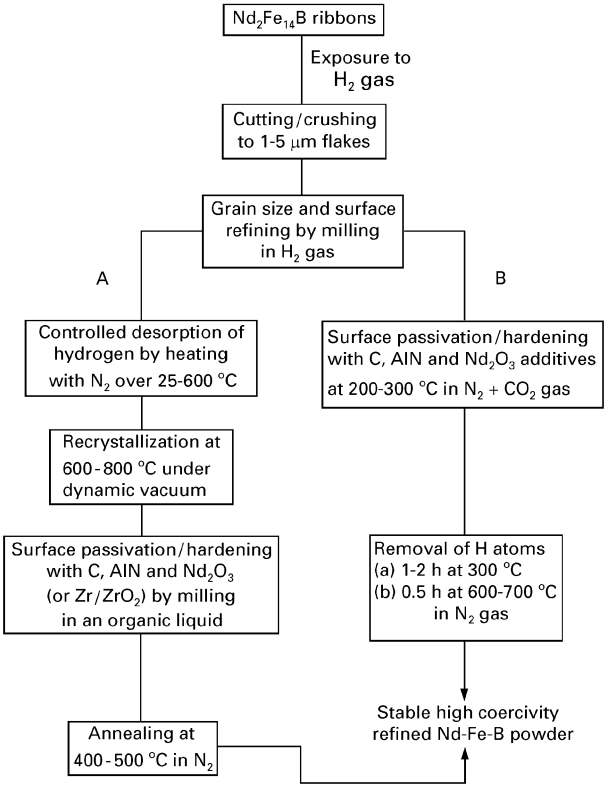

Figure 9 Schematic diagram of mechanical attrition and gas passivation process for the production of high-coercivity refined $Nd_2Fe_{14}B$ powders.

J_r. The high H_{ci} monotonically drops to the original Co free value at $x \approx 0.2$ and then linearly decreases as a function of x, basically governed by the H_a value, which is lowered by the cobalt substitution [9]. We therefore selected $x \approx 0.2$ as the optimal Co substitution to balance a reasonably lowered temperature coefficient $\partial M_s/\partial T$ of M_s by reasonably improved T_C, suitable for the practical applications of high-energy-density magnets with constant M_s and other magnetic parameters over a wide range of temperatures (0–50 °C). A further improvement in H_{ci} is possible through adjustments to the Nd concentrations of 14 at % or higher.

Cobalt-substituted $Nd_2Fe_{14-x}Co_xB$ alloy is more stable and corrosion resistant in open air at room temperature. A typical $Nd_{15.5}Fe_{63.0}Co_{16.0}B_{5.5}$ composition, having a moderate 9.0 wt % excess Nd, thus minimized the M_s loss in air at 14%, with initial $M_s \approx 155\ emu\ g^{-1}$, and beneficially enhanced the T_C value from 310 °C (320 °C for $Nd_2Fe_{14}B$ single crystals) to 450 °C. Fig. 8 compares thermomagnetograms of these samples measured under a magnetic field of 2 kOe. It is found that the small $Nd_2Fe_{14}B$ grains of about 0.14 μm had 2–5% lower T_C values than those for the regular size of about 1 μm or larger. In fact, the small grains have an effectively different magnetic spin distribution on the surface (than below the surface) so that it dilutes the total exchange interactions and thus lowers the T_C value, as we observed and modelled in the W-type hexagonal ferrites [33].

The well-crystallized $Nd_{15.5}Fe_{63.0}Co_{16.0}B_{5.5}$ ribbons with grains as small as about 1 μm present reasonably stable magnetic properties. These were easily cut and milled (without a significant surface oxidation) to flakes of 1–5 μm size which then were heated at 150–200 °C in H_2 gas at 1 bar to form the $Nd_2Fe_{14}BH_x$, $x \approx 5$, hydride. Meanwhile, the H_2 gas also hydrides the intergranular phases, if any. They no longer so intimately adhere to and bind $Nd_2Fe_{14}B$ in small clusters of particles. As a result, the specimen becomes brittle and easy to powder it to particles as small as 1 μm or less using a jet milling or high-energy ball milling.

To ensure stability of the refined powder, a total of 5 wt % R_2O_3, carbon and AlN (in 1:2:2 ratio) was admixed by milling the mixture under hexane (using 5% water) and then the resultant material was annealed at 300 °C in N_2 gas at 1 bar. The N_2 gas helps the desorption of the interstitial H atoms in the sample without decomposition. It reacts with the H atoms and forms NH_3 gas according to

$$N_2 + 3H_2 \rightarrow 2NH_3 \qquad (12)$$

at this temperature. The NH_3 gas absorbs ($NH_3 + H_2O \rightarrow NH_4OH$) the oxygen and moisture impurities, if any, in the specimen and the total is easily pumped off through an efficient vacuum pump. Isothermal heating for about 1 h at 300 °C in a closed volume followed by pumping off the interstitial gases over 300–600 °C for 1 h yields a mostly dehydrided specimen. The dehydrided specimen results in a stable high coercivity powder after a further annealing in N_2 gas at 1 bar and 600–700 °C for 30 min and then slowly cooling it in the device to room temperature as summarized in Fig. 9. At 600–700 °C, the Nd-rich intergranular phases segregate through a low-temperature Nd-rich, $L \rightarrow Nd + Nd_2Fe_{17}$, eutectic [6,41] and coat the ferromagnetic $Nd_2Fe_{14}B$ grains (melting point, about 1180 °C) in combination with the additives.

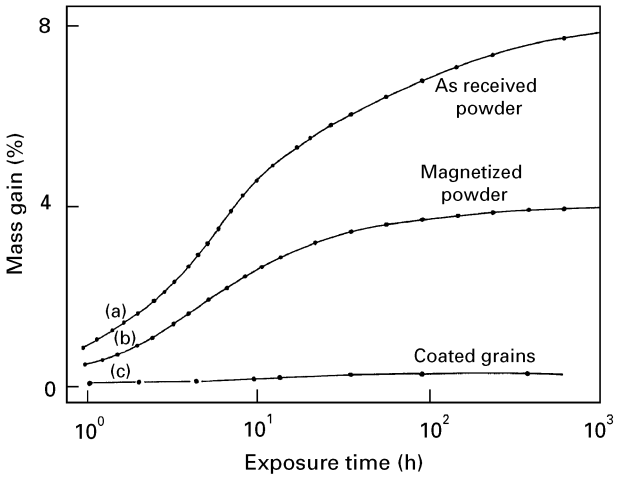

Figure 10 Mass gain of $Nd_{15.5}Fe_{63.0}Co_{16.0}B_{5.5}$ powders during exposure to the laboratory atmosphere: (a) as-received, (b) magnetized and compacted and (c) coated and passivated grain surfaces with carbon and other additives.

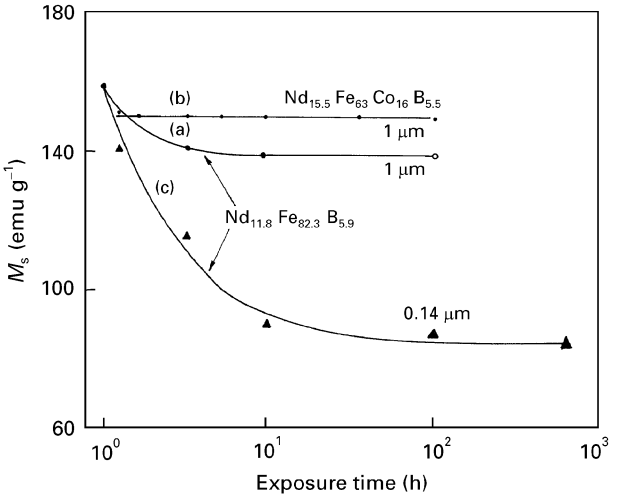

Figure 11 Comparison of M_s loss of fine Nd–Fe–B powders of grain sizes (a), (b) about 1 μm and (c) 0.14 μm. Note the promptly controlled M_s loss in (b) in Co-substituted $Nd_{15.5}Fe_{63.0}Co_{16.0}B_{5.5}$ powder of grain size 1 μm or larger.

The eutectic, if in excess, locally dissolves the expected $NdFe_4B_4$ and other grain-boundary phases and ultimately precipitates them as isolated $Nd_2Fe_{14}B$ grains. It homogenizes the refined microstructure of the specimen. The refined sample is more stable and corrosion resistant in air because it has a much reduced fraction on the intergranular phases which are presumably highly susceptible to oxidation. It hardly shows any mass gain (Fig. 10) or loss in H_{ci} (Fig. 6) or a loss in M_s (Fig. 7) with time on exposure to the laboratory atmosphere. The compacted and sintered magnets of these powders had stable and reproducible magnetic properties. The protective grain-surface passivation film, which was formed rich in the carbides and/or nitrides of the constituent elements, strongly adheres to the grains and does not segregate, particularly if the powder is magnetized and compacted in a desired shape, at room temperature. This is very important for processing and control of the decay of the magnetic properties of the high-quality magnetic powders and their small components and devices in industries.

Our results on the minimal oxidation of the refined particles of about 1 μm (in Fig. 10) are qualitatively similar to those reported by Bogatin *et al.* (cf., Figs 3 and 5 in [13]) for much larger particles of about 10 μm stabilized by milling in water and then gas passivating at 125–300 °C in CO_2 and/or N_2 gas. Of course, the milling in water rapidly oxidizes the small particles of 10 μm or smaller, showing a rapid decrease in the high H_{ci} value from a value of several kilo oersteds to almost zero, as we discussed in [14]. The high H_{ci} value in this case does not recover on thermal annealing and gas passivation. In this case, a limited milling under hexane (or any other similar non-reactive organic liquid with the sample) with about 5% water, as we discussed in the experimental section, is useful to obtain a stable high-H_{ci} refined R-Fe-B powder.

The prescribed additives of carbon and nitrides do not form such a stable grain-surface passivation film on small $Nd_2Fe_{14}B$ grains of about 0.5 μm or smaller. As a result, the specimens of $Nd_{11.8}Fe_{82.3}Co_{16.0}B_{5.9}$ or $Nd_{15.5}Fe_{63.0}Co_{16.0}B_{5.5}$ alloy exhibit a reasonably stable M_s (in Fig. 10a or b) for approximately 1 μm grains but the same alloy with small (about 0.14 μm) grains (in Fig. 10c) have a regularly decreasing M_s value with time in an ambient atmosphere. The additives in small particles rather support the oxidation. The M_s value in Fig. 10c therefore decreased more rapidly from 159 emu g^{-1} to 84 emu g^{-1} (from 165 emu g^{-1} to 95 emu g^{-1} otherwise in Fig. 7a) within the first 4 months exposure in an ambient atmosphere by which time the effect has saturated. As soon as fresh $Nd_2Fe_{14}B$ grain surfaces are exposed to air, they readily oxidize with oxygen or moisture, showing a concomitantly increasing mass of the specimen on a balance. The reaction begins with Nd atoms. The oxidized Nd atoms segregate and coat the grains in a characteristically whitish-pink colour of $Nd(OH)_3$ or NdOOH. We carefully studied several specimens with fresh grain surfaces. The Nd was found always to precipitate first and then to spread over the grains as a further oxidation-protective oxide layer. The process of the oxidation and stabilization of the oxide layer is modified in an aqueous medium. In this case, the Fe atoms in the $Nd_2Fe_{14}B$ grains go on oxidizing and do not allow the oxidation-protective layer to form and stabilize.

3.4. H-induced lattice disordering and recrystallization of anisotropic $Nd_2Fe_{14}B$ particles

It is worth mentioning that the Nd–Fe–B powders pulverized from the optimally quenched ribbons by the above methods do not exhibit a perfect rectangular hysteresis loop expected in an assembly of anisotropic grains. In Fig. 12a, the magnetization rather rapidly decreases between points A and B and forms a distorted rectangular hysteresis loop with a rather low $J_r = 8.12$ kG, but a high $H_{ci} = 17.12$ kOe value. This means that some of the grains are still sticking together with different orientations of their easy axes

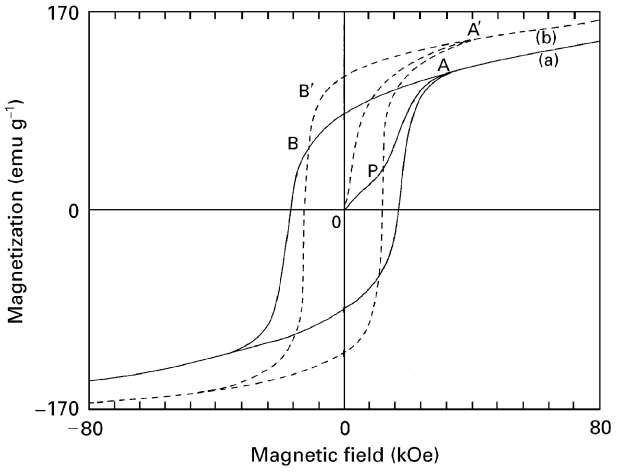

Figure 12 Hysteresis loops of (a) 1–5 μm flakes and (b) recrystallized $Nd_{15.5}Fe_{63.0}Co_{16.0}B_{5.5}$ powder.

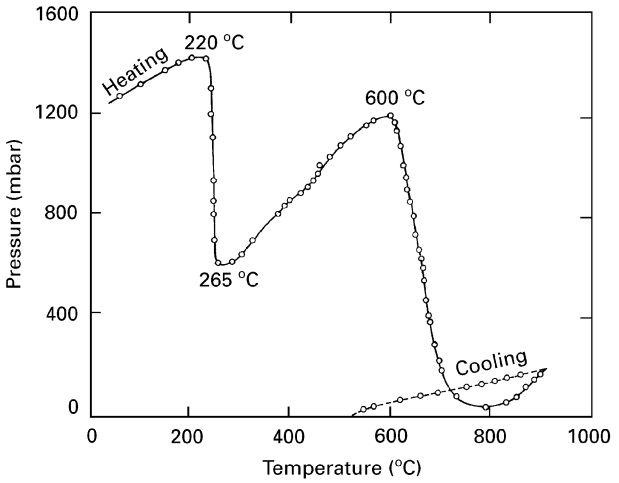

Figure 13 Reaction of H_2 gas with 1–5 μm $Nd_2Fe_{14}B$ flakes during heating in a closed volume.

of magnetization. It can be improved by recrystallizing the refined powder by a hydrogen decrepitation (HD) or hydrogen disproportionation desorption recombination (HDDR) process as discussed elsewhere [23]. Here, we use similar methods in combination with grain-surface passivation (or surface hardening) with particular non-magnetic additives to obtain stable high-coercivity Nd–Fe–B powders as follows.

As summarized in Fig. 9, the Nd–Fe–B alloy absorbs the interstitial H atoms at 150–200 °C and forms isostructural ($P4_2/mnm$ tetragonal crystal structure) hydrides by an expansion of the crystal lattice of up to 4.2%. In isochronal heating (5 °C min^{-1}), a typical specimen (in Fig. 13) of 1–5 μm flakes over 25–900 °C in H_2 gas at about 1 bar (initial pressure), the gas pressure linearly increases with increasing temperature, according to the $PV = RT$ gas law, but rapidly drops at around 220 °C (depending on the rate of the heating), hydriding the $Nd_2Fe_{14}BH_x$, $x \leqslant 5$, sample. At higher temperatures, some of the H atoms desorb, mostly between 250 and 450 °C, and accumulate in the reaction chamber up to the equilibrium pressure. The gas pressure again sharply drops at around 600 °C, performing an H-induced thermal decomposition–transformation of the specimen according to

$$Nd_2Fe_{14}BH_x + \beta H_2 \xrightarrow{600\,^\circ C,\ H_2} 2NdH_{2+\delta} + (Fe_2B + 12Fe) \quad (13)$$

with $\beta + x/2 = 2 + \delta$ and $\delta \leqslant 1$. Depending upon the experimental conditions, the product results in an X-ray amorphous or nanocrystalline mixture with nanocrystalline α-Fe. The result is consistent with the previous reports using the HD or HDDR processes [23, 42]. At this temperature, the $Nd_2Fe_{14}B$ grain surface acts as a very efficient catalyst to dissociate the H_2 molecules into H atoms, which instantly react with the Nd atoms by dissociating the alloy and form $NdH_{2+\delta}$, $\delta \leqslant 1$, hydrides. Production of such refined powders of this alloy is not so easily possible by mechanical attrition or other similar methods.

Recrystallization of the refined powder in Equation 13 occurs on heating at 700–800 °C under a dynamic vacuum and results in a refined microcrystalline $Nd_2Fe_{14}B$ powder. Grains as small as a few hundred nanometres thus have been formed during heating for 30 min at 700–800 °C followed by rapidly cooling in the device. The present experiment differs from the previous report with the HDDR process [23] in the sense that it does not use the final heating under vacuum. Under the dynamic vacuum, the $NdH_{2+\delta}$ in the refined sample slowly desorbs the hydrogen over these temperatures and allows the latter to recombine simultaneously with the Fe and B components of the alloy in the sample to re-form the separated anisotropic $Nd_2Fe_{14}B$ particles. Strictly speaking, the re-formation of the separated anisotropic $Nd_2Fe_{14}B$ particles in this example occurs better under a dynamic vacuum than that in a pure vacuum. The experiment performed under vacuum yields reasonably large polycrystalline $Nd_2Fe_{14}B$ grains which never exhibit a rectangular hysteresis loop characteristic of separated single-domain ferromagnetic particles.

A small (about 5%) addition of a dispersoid mixture of R_2O_3 (or $Zr–ZrO_2$), carbon and AlN (in 1:2:2 ratio) during the recrystallization reaction in this example inhibits the growth of large $R_2Fe_{14}B$ grains by inhibiting the recombination reaction between the separated grains. The sample of separated crystallized grains exhibits a rectangular hysteresis loop (Fig. 12b). The separated $Nd_2Fe_{14}B$ grains magnetize by a regular displacement and rotation of the domain walls as a function of the applied magnetic field. A regular magnetization therefore occurs between points O and A′ in the first quadrant of the magnetization in Fig. 12b. Otherwise, the magnetization (cf., Fig. 12a) relatively slowly increases over the low fields and shows a discontinuity in it at point P.

A recrystallized $Nd_{15.5}Fe_{63.0}Co_{16.0}B_{5.5}$ powder, using a partial substitution of Co on the Fe sites in $Nd_2Fe_{14}B$, thus measures a dramatically enhanced (about 45%) $J_r = 11.8$ kG together with an approximately 28% lowered $H_{ci} = 12.40$ kOe so that the area under the hysteresis loop remains the same as in the starting sample. The recrystallization involves co-precipitation of 2–5 wt % iron, presumably from the

intergranular phases, showing an approximately 13% increase in the total M_s value (with the final $M_s = 175\ \text{emu g}^{-1}$) of the sample at room temperature. These iron impurities, which were identified by the X-ray diffractogram, exhibit a well-defined T_C at 760 °C (768 °C in pure iron) in the thermomagnetogram. It is to be noted that iron is a basically soft magnetic material. It exhibits an extremely small $H_{ci} \leqslant 50$ Oe but a high $M_s = 217.5\ \text{emu g}^{-1}$ value at room temperature. However, in this example, it does not maintain its independent identity. The $Nd_2Fe_{14}B$ sample with the Fe impurities, therefore, maintains a symmetric shape of the hysteresis loop. These iron impurities seem to be strongly magnetically coupled with the ferromagnetic $Nd_2Fe_{14}B$ grains which govern the magnetization of the coupled Fe nanoparticles (which magnetize usually over relatively low fields (0–10 kOe or so)) by the local magnetic fields of the separated $Nd_2Fe_{14}B$ grains. This is a very important process parameter to explore a high M_s or J_r value in the high-energy-density R–Fe–B composite magnets using the coupled soft magnetic impurities with the hard ferromagnetic $R_2Fe_{14}B$ grains.

The recrystallized Nd-Fe-B alloy powder, without the grain-surface passivation with the non-magnetic additives, is rather highly reactive to oxygen or moisture in an ambient atmosphere but can be stored under a pure argon gas or acetone or a similar non-oxidizing organic liquid. It was used to fabricate zinc-bonded magnets by mixing, magnetically aligning and compacting with a total of 30 wt % addition of zinc and carbon (in 10:1 ratio) and then heating the resultant material at 400–500 °C (with intermediate compactions) for 3 h in a pure argon. The magnets made in this way had stable magnetic properties of $J_r = 10.8$ kG, $H_{ci} = 13$ kOe and $(BH)_{max} \approx 31$ MG Oe.

3.5. Stable $Nd_2Fe_{14}B$ powders through chemical routes

A technical advantage of the $Nd_2Fe_{14}B$ powders co-reduced by calcium (a reducing agent) is that the byproduct (CaO) intimately coats the individual $Nd_2Fe_{14}B$ grains during the reaction at 900–1000 °C [6]. That protects the $Nd_2Fe_{14}B$ grains with oxidation in water in a subsequent step of washing the mixture in water at room temperature. The water thus washes away the byproducts without significantly oxidizing the sample. A sample of $Nd_2Fe_{14}B$ grains as small as about 1 μm thus had formed an oxidized grain-surface layer only about 0.04 μm thick (which was estimated from the difference between the magnetic moment of the sample and that for a pure $Nd_2Fe_{14}B$ sample) during the washing process as summarized in Fig. 14. This thin layer becomes rigidly hard and oxidation proof on immediately drying the recovered powder under vacuum at 50–100 °C. It then prevents further oxidation of the sample in an ambient atmosphere. This sample, therefore, has been found to be substantially stable. It can be stored in a laboratory air atmosphere for an extended period of time with no further loss in its structural or magnetic properties.

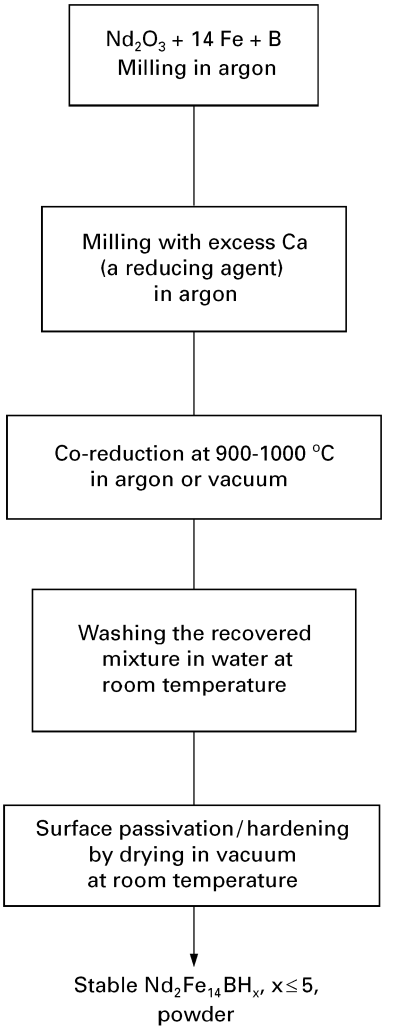

Figure 14 Schematic diagram of synthesis of stable $Nd_2Fe_{14}BH_x$, $x \leqslant 5$, powders by co-reduction reaction with calcium metal (a reducing agent).

The above-mentioned alloy powder is more or less always hydrided to $Nd_2Fe_{14}BH_x$, $x \leqslant 5$, by the nascent hydrogen produced by chemical dissociation of the water on the highly reactive grain-surfaces of $Nd_2Fe_{14}B$ or residual Ca, if any, in the reaction mixture, during washing the mixture in water:

$$\begin{aligned} Nd + 3H_2O &\rightarrow Nd(OH)_3 + 3H \\ Fe + 3H_2O &\rightarrow Fe(OH)_3 + 3H \\ Ca + 2H_2O &\rightarrow Ca(OH)_2 + 2H \end{aligned} \qquad (14)$$

The nascent hydrogen very efficiently reacts with the sample under the present conditions and forms the hydrides. Four main interstitial sites of the H atoms in the sample have been identified by selective thermal desorption of the H atoms [43]. The amount of hydrogen, x, utilized in hydriding the specimen depends purely on the experimental conditions, i.e., on firstly the amount of the H_2 produced in the reaction, secondly on the amount of unoxidized calcium in the mixture, thirdly on the way that the $Nd_2Fe_{14}B$ crystallites are coated in the byproducts, and fourthly on the way that the mixture is washed in cold water. Thus an appropriately co-reduced mixture of Nd_2O_3, Fe and B using 100% excess Ca (with respect to that required in the primary $Nd_2O_3 + 3Ca \rightarrow 2Nd$

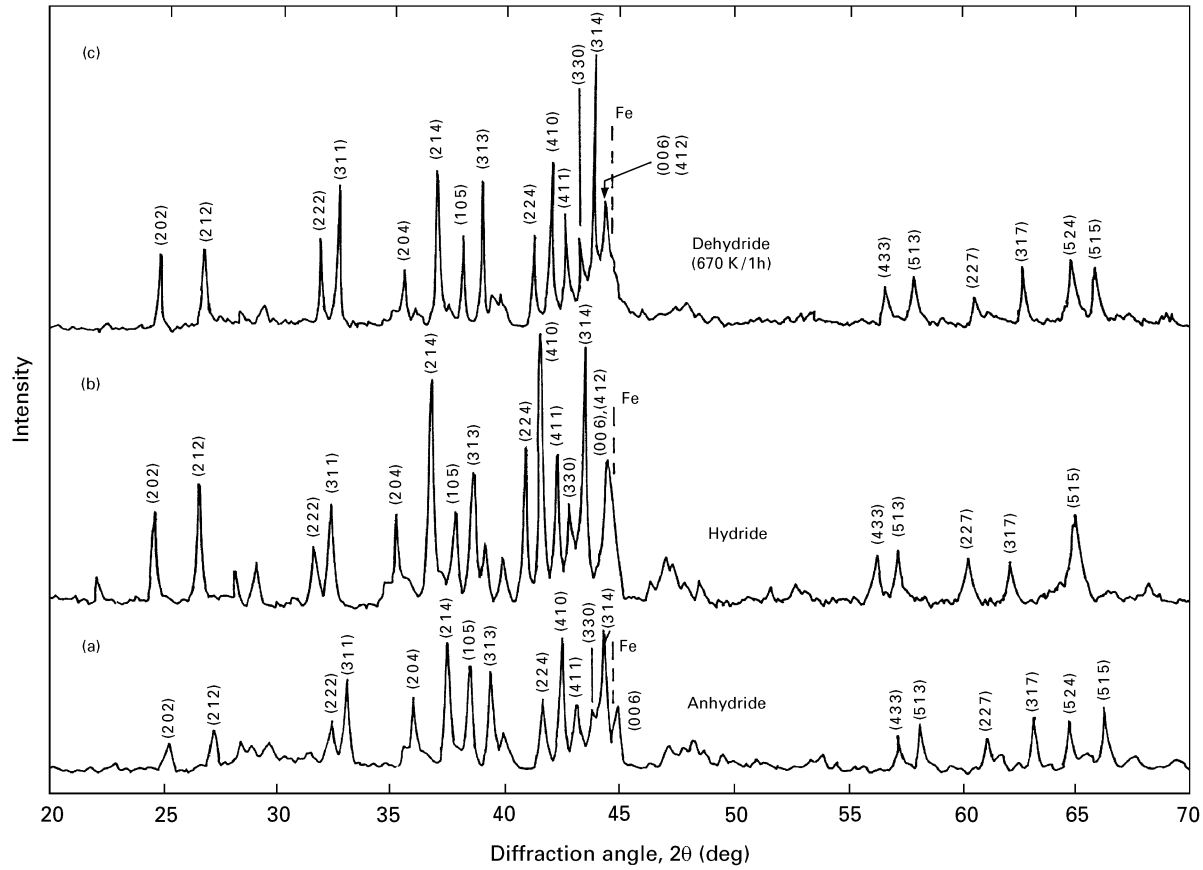

Figure 15 X-ray diffraction patterns of (a) anhydride and (b) $Nd_2Fe_{14}BH_x$, $x \approx 4$, hydride powders co-reduced by calcium and washed in cold water. Diffractogram (c) is taken after dehydriding (b) at about 400 °C. The broken line at 2.0268 Å indicates the expected position of the $\alpha - Fe$ impurity line, if any.

+ 3CaO reduction reaction) and then washing it in a limited amount of cold water in a closed confined volume at room temperature (prior to repeatedly washing in fresh large amounts of water) easily yields a saturated $Nd_2Fe_{14}BH_x$, $x \approx 5$, hydride [18]. Both hydride and anhydride samples have essentially the same X-ray diffraction patterns (Fig. 15), except a minor change in the intensity distribution for some peaks and a regular shift in all the characteristic peaks over lower 2θ (larger d_{hkl}) values in the hydride in the expected 4.2% expansion in the crystal lattice. All the peaks in either case are well indexed assuming the same $P4_2/mnm$ tetragonal crystal lattice with the lattice parameters $a = 8.93$ Å and $c = 12.32$ Å for the hydride and $a = 8.80$ Å and $c = 12.18$ Å for the anhydride.

The present diffractograms (Fig. 15) compare fairly well with those for the rapidly quenched $Nd_{14.5}Fe_{80.0}B_{5.5}$ ribbons in Fig. 2. The (410) reflection at $d_{hkl} \approx 2.31$ Å appears to be the most intense in either sample with a grain size of about 1 μm. The intensity distribution in the characteristic $Nd_2Fe_{14}B$ lines is somewhat modified in the samples with smaller grains. This is possible if the grains in the sample have a preferred orientation. As a result, a sample of approximately 0.14 μm $Nd_2Fe_{14}B$ grains (in Fig. 2b) exhibits a maximum intensity in the (214) reflection, which is the second most intense line in the other sample (Fig. 2c), at $d_{hkl} \approx 2.41$ Å. Moreover, the (314) reflection at $d_{hkl} \approx 2.05$ Å becomes the most intense on partially dehydriding the hydride powder (Fig. 15c) at 400 °C. A complete desorption of the total H atoms in the sample is not possible at this temperature. The dehydrided sample at 400 °C thus retains a larger lattice volume $V = 957 \times 10^{-24}$ cm^3 and a larger $T_C = 340$ °C than $V = 943 \times 10^{-24}$ cm^3 and $T_C = 320$ °C (369 °C in the saturated $Nd_2Fe_{14}B$ hydride) for the anhydride.

The water-washed (and subsequently dried under vacuum at ~300 K)$Nd_2Fe_{14}B$ hydride, which is substantially stable with stable grain-surface passivation in ambient atmosphere and which exhibits a very low $H_{ci} \approx 0$ value, with the usual $M_s = 145$ emu g^{-1} value, seems to be particularly useful for magnetic recording heads and other applications of extremely soft magnetic materials. The H_{ci} value is somewhat improved up to a value of 5–10 kOe together with a high value for $J_r = 10$–12 kG or $M_s = 165$ emu g^{-1} on a controlled thermal desorption of the H atoms and then annealing the sample at 700–800 °C with 5 wt % addition of AlN and carbon as discussed above. The sample in this example directly results in a stable, finely divided loose magnetic powder of well-separated grains of size on a submicrometre scale. No further finishing of the microstructure is needed in order to fabricate the sample into a permanent magnet and other components and devices.

4. Conclusions

A combination of rapid quenching and high-energy mechanical attrition is explored to synthesize stable

$R_2Fe_{14}B$ powders of isolated submicrometre-sized grains with minimal intergranular phases, which are rather highly susceptible to unwanted oxidation and corrosion in air. Such small (high-surface-energy) grains of pure R–Fe–B alloy, without an external grain-surface coating or protection, behave in a highly pyrophoric manner and catch fire in open air at room temperature. On milling 1–5 μm flakes of the sample (cut from thin ribbons of the sample obtained by rapid quenching) under an appropriate organic liquid (to cause no excess oxidation of the sample), the presumed intergranular phases, which are softer than the primary phase, segregate and coat the separated $R_2Fe_{14}B$ grains. The resulting $R_2Fe_{14}B$ grain surfaces very efficiently adsorb and react with the additives of carbon, AlN and R_2O_3 (by milling followed by annealing at 300–700 °C in N_2 gas), forming a stable $R_2Fe_{14}B$ grain-surface film rich in the carbide or nitride of the elements involved.

In ambient atmosphere, a fast oxidation reaction of the O_2 or H_2O with the R atoms (which have a characteristically high oxidation potential, ϕ, e.g., $\phi = -2.41$ V for Nd) in the $R_2Fe_{14}B$ grain surfaces is the main driving force for oxidizing the sample. The $R_2Fe_{14}B$ grain-surface treatments and passivation with the above additives (in the presence of N_2 gas), in principle, function on similar but controlled oxidation reactions so that the reaction products, which are nanocomposites of the carbides or nitrides of R or Fe, iron (or iron oxides) and oxidized R, form a thin, thermally rigid $R_2Fe_{14}B$ surface passivation layer. It cuts off the chemical driving force for further oxidation of R atoms in the bulk and stabilizes the $R_2Fe_{14}B$ grains by controlled surface oxidation passivation. This grain-surface passivation layer is only a few nanometres thick but behaves rigidly and protects the specimen from further oxidation in air at room temperature.

In particular, the $R_2Fe_{14}B$ grain-surface passivation film stabilized with so-called R-rich intergranular phases, if any, behaves as non-magnetic compared with the primary ferromagnetic phase. It keeps the grains separated and inhibits mixing between the local magnetic lines of forces confined to the separated $R_2Fe_{14}B$ grains. As a result, the r_c-sized single-domain $R_2Fe_{14}B$ grains presumably behave as ideally single-domain anisotropic magnetic particles, showing a rectangular hysteresis loop with a reasonably high value of $H_{ci} = 10$–25 kOe. In the absence of the non-magnetic layers, the domain walls in the highly magnetic $R_2Fe_{14}B$ grains run non-interrupted from grain to grain, forming an extended domain structure, through several grains. Thus even the small grains of $r \leqslant r_c$ geometrical sizes ultimately behave as magnetically multiple-domain grains. They, therefore, contribute a characteristically low H_{ci} value.

Several Nd–Fe–B compositions, including a partial substitution of Fe by Co have been studied, and, in particular, their magnetic properties and thermal stability characterized for high-energy-density magnets and other magnetic and electronic applications. The compositions, having a small (about 0.4%) substitution of Co in the Fe sites (in $R_2Fe_{14}B$) together with 5–10 wt % excess Nd (over the $R_2Fe_{14}B$ composition) have been found to exhibit reasonably stable reproducible magnetic properties with reasonably improved T_C values. Thermal treatments and grain-surface refinement with particular carbide and/or nitride additives supports the grain-surface hardening and stability of the sample against atmospheric corrosion. A small 5–10% replacement of Nd by Pr in these compositions is advised to obtain a suitably thicker stable $R_2Fe_{14}B$ grain-surface protective layer.

The excess Nd (or Pr) forms the presumed R-rich intergranular phases, which are basically non-magnetic compared with the ferromagnetic $R_2Fe_{14}B$ phase. The advantage of this is that they considerably improve the H_{ci} value but adversely lower the total magnetic moment of the specimen. Moreover, they are highly susceptible to oxidation. They cause $R_2Fe_{14}B$ lattice instabilities in presence of the small impurities such as oxygen atoms. Nevertheless, they form a low-temperature $L \rightarrow Nd + Nd_2Fe_{17}$-type eutectic [6, 9]. As a result, they behave as reasonably mechanically soft materials on heating the sample at 300–700 °C under N_2. It helps to perform the $R_2Fe_{14}B$ grain-surface passivation (or surface hardening) with suitable non-magnetic high-temperature additives of carbon, BN or AlN. At this temperature, they help the additives to diffuse into the highly reactive $R_2Fe_{14}B$ grain surfaces by causing grain-surface hardening and stable grain-surface passivation in combination with the additives. It is not clear how the N_2 gas here helps in the stabilization of the grain-surface passivation but it clearly results in a minimal increase in the average magnetic moment of the sample by up to about 2% together with a 3–10% increase in the Curie temperature, which are useful for several applications of high-energy-density magnets and related devices and components.

Acknowledgements

The author gratefully acknowledges the personal discussions with Professor J.C. Joubert (Domaine Universitaire, Saint-Martin d'Héres, France) and Professor H.J. Fecht (Institute of Metal Research, Technische Universität Berlin), and the financial support from the AvH Foundation, Germany.

References

1. K. D. DURST and H. KRONMÜLLER, *J. Magn. Magn. Mater.* **68** (1987) 63.
2. O. KUBO, T. IDO, H. YOKOYAMA and Y. KOIKE, *J. Appl. Phys.* **57** (1985) 4280.
3. T. FUJIWARA, *IEEE Trans. Magn.* **21** (1985) 1480.
4. S. RAM, *J. Magn. Magn. Mater.* **82** (1989) 129.
5. S. RAM and J. C. JOUBERT, *IEEE Trans. Magn.* **28** (1992) 15.
6. *Idem., J. Appl. Phys.* **72** (1992) 1164.
7. J. F. HERBST, J. J. CROAT, F. E. PINKERTON and Y. B. YELLON, *Phys. Rev. B* **29** (1984) 4176.
8. M. SAGAWA, S. FUJIMURA, M. TOGAWA and Y. MATSUURA, *J. Appl. Phys.* **55** (1984) 2083.
9. K. J. H. BUSCHOW, *Mater. Sci. Rep.* **1** (1986) 1.
10. L. SCHULTZ, J. WECKER and E. HELLSTERN, *J. Appl. Phys.* **61** (1987) 3583.

11. L. SCHULTZ, K. SCHNITZKE and J. WECKER, *ibid.* **64** (1988) 5302.
12. K. SCHNITZKE, L. SCHULTZ, J. WECKER and M. KATTER, *Appl. Phys. Lett.* **56** (1990) 587.
13. Y. BOGATIN, M. ROBINSON and J. ORMEROD, *J. Appl. Phys.* **70** (1991) 6594.
14. E. CLAUDE, S. RAM, I. GIMENEZ, P. CHAUDOUET, D. BOURSIER and J. C. JOUBERT, *IEEE Trans. Magn.* **29** (1993) 2767.
15. F. E. PINKERTON and C. D. FUERST, *J. Magn. Magn. Mater.* **89** (1990) 139.
16. R. E. CECH, US Patent 3 625 779 (1971).
17. *Idem.*, *J. Metals* **26** (1974) 32.
18. S. RAM and J. C. JOUBERT, *Appl. Phys. Lett.* **61** (1992) 613.
19. S. RAM, E. CLAUDE and J. C. JOUBERT, *IEEE Trans. Magn.* **31** (1995) 2200.
20. Ph. l'HERITIER, P. CHAUDOUET, R. MADAR, A. ROUAULT, J. P. SENATEUR and R. FRUCHART, *C.R. Acad. Sci., Paris, II* **299** (1984) 849.
21. J. M. CADOGAN and J. M. D. COEY, *Appl. Phys. Lett.* **48** (1986) 442.
22. L. PARETI, O. MOZE, D. FRUCHART, P. l'HERITIER and Y. YAOUANE, *J. Less-Common Metals* **142** (1988) 187.
23. I. R. HARRIS and P. J. McGUINESS, *ibid.* **172-4** (1991) 1273.
24. X. J. YIN, I. P. JONES and I. R. HARRIS, *J. Magn. Magn. Mater.* **125** (1993) 91.
25. J. I. LANGFORD, *J. Appl. Crystallogr.* **11** (1978) 10.
26. J. W. CHRISTIAN, "The theory of transformation in metals and alloys" (Pergamon, Oxford, 1975).
27. H. A. DAVIES, A. MANAF, M. LEONOWICZ, P. Z. ZHANG, S. J. DOBSON and R. A. BUCKLEY, *Nano-Struct. Mater.* **2** (1993) 197.
28. Y. MATSUURA, S. HIROSAWA, H. YAMAMOTO, S. FUJIMURA, M. SAGAWA and K. OSAMURA, *Jpn. J. Appl. Phys.* **24** (1985) L635.
29. E. STONER and E. WOHLFARTH, *Phil. Trans. R. Soc. A* **240** (1948) 599.
30. C. D. MEE and J. C. JESCHKE, *J. Appl. Phys.* **34** (1963) 1271.
31. B. T. SHIRK and W. R. BUESSEM, *ibid.*, **40** (1969) 1294.
32. *Idem.*, *J. Amer. Ceram. Soc.* **53** (1970) 192.
33. S. RAM and J. C. JOUBERT, *Phys. Rev. B* **44** (1991) 6825.
34. S. HIROSAWA, Y. MATSUURA, H. YAMAMOTO, S. FUJIMURA, M. SAGAWA and H. YAMAUCHI, *J. Appl. Phys.* **59** (1986) 873.
35. M. C. D. DERUELLE, M. YAMADA, H. YAMAUCHI and Y. NAKAGAWA, *Phys. Rev. B* **42** (1990) 10 291.
36. D. W. LIM, H. KATO, M. YAMADA, G. KIDO and Y. NAKAGAWA, *ibid.* **44** (1991) 10 014.
37. K. TOKUHARA, Y. OHTSU, F. ONO, O. YAMADA, M. SAGAWA and Y. MATSUURA, *Solid State Commun.* **56** (1985) 333.
38. M. FOLDEAKI, L. KOSZEGI and R. A. DUNLAP, *J. Magn. Magn. Mater.* **96** (1991) 29.
39. D. X. CHEN, V. SKUMRYEV and H. KRONMÜLLER, *Phys. Rev. B* **46** (1992) 3496.
40. C. D. FUERST and J. F. HERBST, *J. Appl. Phys.* **66** (1989) 1782.
41. G. SCHNEIDER, G. MARTINEK, H. H. STADELMAIER and G. PETZOW, *Mater. Lett.* **7** (1988) 215.
42. S. RAM, M. FEBRI, H. J. FECHT and J. C. JOUBERT, *Nano-struct. Mater.* **6** (1995) 473.
43. S. RAM, *Phys. Rev. B* **49** (1994) 9632.

Received 15 September 1995
and accepted 19 December 1996